Magnetic Biomorphic $BaFe_{12-x}Cr_xO_{19}$ Ceramics with Multilayer Wall Structure Made from Spruce Templates

Rui Li,[a,b] Zuju Shu,[a,c] Liangcun Qian,[a,b] Liang Zhou,[a] Yamei Liu,[a] and Shengquan Liu [a,*]

$BaFe_{12-x}Cr_xO_{19}$ (x = 0.0, 0.1, 0.2, 0.3, and 0.4) ferrite ceramics were prepared by a sol-gel method using spruce sapwoods as the templates. The prepared materials were characterized by scanning electron microscopy (SEM), X-ray diffraction (XRD), and a magnetic property measurement system (MPMS). The prepared materials maintained a multilayer wall structure of spruce sapwoods. All samples presented the single-phase of the magnetoplumbite barium hexaferrite. The saturation magnetization initially increased until it reached a maximum value at x = 0.2 and then decreased in three directions (parallel cross section, parallel radial section, and parallel tangential section). The coercivity decreased monotonously when measured in three directions. However, the coercivity was obviously lower in the parallel cross section direction than in the other directions because of the structural anisotropy caused by the multilayered wall structure.

Keywords: Multilayer wall structure; $BaFe_{12-x}Cr_xO_{19}$; Cr^{3+}; Magnetic properties

Contact information: a: College of Forestry and Gardening, Anhui Agricultural University Hefei, 230036, P.R. China; b: School of Science, Anhui Agricultural University Hefei, 230036, P.R. China; c: School of Textile Engineering and Art, Anhui Agricultural University Hefei, 230036, P.R. China;
** Correspondence author: Liusq@ahau.edu.cn*

INTRODUCTION

Materials produced by land-based plants or lignocellulosics, such as wood, palms, crops, grasses, and vegetable fibres, are natural bio-organic composites that often exhibit porous, anisotropic morphologies. The first wood-based ceramics were made in the late 1990's using silicon carbide (Ota *et al*. 1995). Many other ceramics such as TiO_2 ceramics (Qian *et al*. 2015), Al_2O_3 ceramics (Liu *et al*. 2006), and $Sr_3Co_2Fe_{24}O_{41}$ ceramics (Pullar *et al*. 2015) have been made since then. These materials feature excellent strength at a low density and high stiffness and elasticity (Okada *et al*. 2011). The morphology of such bio-organic material consists of a hierarchical system, ranging in size from millimeters (growth ring patterns in wood) to microns (cellulose fibres, wood cells). This hierarchical architecture has a cellular microstructure of high porosity, characteristic to the specific function of living cells, such as the transportation of water and gases, storage, and mechanical strength. These cells form a system of pore-like channels, with preferential orientation along an axial direction. This feature offers the possibility of using liquid infiltration techniques, either to fill these pores with liquid to form a "negative" microstructure of the original wood, or to impregnate the actual cellular structure of the wood and transform it into an inorganic copy of the original cellular structure (Ohji and Fukushima 2012; Birol *et al*. 2013). Structural templates allow for the creation of a large variety of biomimetic materials, which maintain the structural integrity

of wood and include carbides, oxide ceramics, and composites with tailored chemical, physical, and mechanical properties (Hübert *et al*. 2009; Van Opdenbosch *et al*. 2010).

The hexaferrites were first made by Philips in the 1950's. These important magnetic materials have numerous applications in microwave devices, high density recording media, magneto-optic media, electric motors, and magnetic heads (Durmus *et al*. 2014; Hosseini *et al*. 2015; Kaur *et al*. 2015). Several synthesis techniques have been used to prepare and tailor the properties of barium hexaferrite nanoparticles. Barium hexaferrite crystallize in a hexagonal structure, the unit cell consists of two compound molecules and contains 24 iron (Fe) atoms. The 24 iron (Fe) atoms are distributed over five distinct interstitial sites: three octahedral sites (12k, 2a, and $4f_2$), one tetrahedral site ($4f_1$), and one bi-pyramidal site (2b) (Töpfer *et al*. 2015). The electrical and magnetic properties of M-type hexa-ferrites can be tailored using different dopants on these interstitial sites. When other ions are incorporated into the structure of BaM, the saturation magnetization, coercivity, anisotropy field, and magnetic resonance frequency will change.

Barium hexaferrite nanoparticles was well-known as a traditional microwave absorber. However, the weight ratios of the ferrite powders in the microwave absorbing coating are usually high (60% to 80%). Compared with the barium hexaferrite nanoparticles, the porous barium hexaferrite ceramics might be more suitable to be applied in electro-magnetic interference due to its low density. This study investigated a sol-gel synthesis method for spruce-templated $BaFe_{12-x}Cr_xO_{19}$ ceramics, with a retained multilayer wall structure from a natural spruce template. The element Cr^{3+} was selected for substituting the Fe^{3+} ions. The effects of the multilayer wall structure, doping on the phase composition, and the morphology and magnetic properties of $BaFe_{12-x}Cr_xO_{19}$ ceramics were examined.

EXPERIMENTAL

Materials

$Ba(NO_3)_2$, $Fe(NO_3)_3 \cdot 9H_2O$, $Cr(NO_3)_3 \cdot 9H_2O$, $C_6H_8O_7 \cdot H_2O$, and NH_4OH were supplied by the Sinopharm Chemical Reagent Co., Ltd., Shanghai, China. All reagents were analytical grade and used without further purification. Spruce samples were obtained from Yingyang Forest Farm in Pingxiang County of the Guangxi Zhuang autonomous region in China.

Methods

Wood sample preparation

Spruce specimens were cut into rectangular specimens of 6 mm (axial) × 8 mm (radial) × 8 mm (tangential). The preforms were extracted using a Soxhlet apparatus with a 2:1 toluene-ethanol solution for 12 h. The specimens were boiled in distilled water for 3 h and dried at 110 °C for 6 h.

Barium ferrite sol preparation

$Ba(NO_3)_2$, $Fe(NO_3)_3 \cdot 9H_2O$, and $Cr(NO_3)_3 \cdot 9H_2O$ were weighed according to the required stoichiometric proportion for $BaFe_{12-x}Cr_xO_{19}$ (x = 0 to 0.4) and mixed at 60 °C for 30 min with stirring. The chelating agent $C_6H_8O_7 \cdot H_2O$ was added, and the solution

was stirred for an additional 30 min. Finally, the sol was adjusted to neutral pH using NH_4OH. The solution was allowed to evaporate on a hot plate at 70 to 80 °C (solution temperature) with continuous stirring until the appropriate concentration of sol was obtained.

Biomorphic barium ferrite ceramics preparation

Spruce specimens were immersed for 1 h in the sol in a covered beaker and then placed in a vacuum drying chamber at 60 °C for 48 h. For each batch of extracted spruce pieces, three infiltration cycles were performed using the same infiltration sol. Between each infiltration, the spruce specimens were dried for 24 h at 60 °C in a vacuum drying chamber to remove adherent liquids. Finally, the specimens were calcined at 250 °C for 1 h and then at 1000 °C for 3 h. The heating rate was 2 °C/min.

Characterization

The phase formation during processing was identified using an XD-3 X-ray diffractometer (XRD; Beijing Persee Instrument Co., Ltd, Puxi, China) operating with Cu Kα radiation (λ = 15.40563 nm) with a scan rate of 1°/min, accelerating voltage of 36 KV, applied current of 20 mA, and diffraction angle (2θ) ranging from 20° to 80°. Microstructures in the biomorphic BaFe12-xCrxO19 ceramics were observed using a scanning electron microscope (SEM; S-4800, HITACHI, Tokyo, Japan). The magnetic properties were examined using an MPMS XL-7 magnetic property measurement system (Quantum Design Inc., San Diego, USA). The magnetic field used was 1 T, and the measurement temperatures was 25 °C.

RESULTS AND DISCUSSION

Structural Characteristics

In X-ray diffraction patterns collected from the infiltrated specimens sintered at 1000 °C for 3 h, the well defined, sharp, and intense peaks confirmed the formation of well-crystallized doped ferrites (Fig. 1).

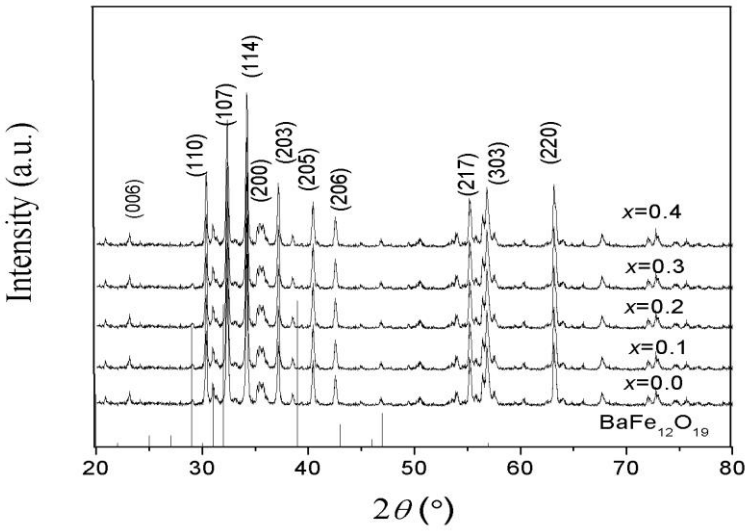

Fig. 1. XRD patterns of $BaFe_{12-x}Cr_xO_{19}$ ceramics sintered at 1000 °C

The diffraction peaks confirmed the formation of a single-phase, hexagonal structure for all samples, without any impurities or secondary phases. Thus, Cr^{3+} entered the barium ferrite in the sub-lattice.

The structural parameters, such as the lattice constants of *a* and *c*, were calculated from the following equation (Gordani *et al*. 2014),

$$d_{hkl} = [\frac{4(h^2 + hk + k^2)}{3a^2} + \frac{l^2}{c^2}]^{-\frac{1}{2}} \quad (1)$$

where *d* is the distance between lattice planes and *h*, *k*, and *l* are Miller indices. The variation of the lattice parameters as a function of *x* are shown in Fig. 2. Increasing the concentration of the dopants in the hexaferrite structure resulted in an almost constant lattice parameter, while the parameter *c* decreased from 23.35 Å to 23.12 Å. The lattice parameter ratio (*c*/*a*) was in the expected range from 3.93 to 3.97 verified the formation of M-type hexagonal ferrite.

Because Cr^{3+} (0.063 nm) and Fe^{3+} (0.064 nm) have similar ionic radii, the decreased lattice constant *c* was not related to the ionic radius. Chromium replaces iron at octahedral sites due to favorable crystal field effects; Cr^{3+} has a field energy of $6/5\Delta_0$ compared with $0\Delta_0$ for Fe^{3+}. Therefore, the lattice constant *c* changed with increasing chromium content, which indicated flattening of the unit cell and a reduction in size (Katlakunta *et al*. 2015).

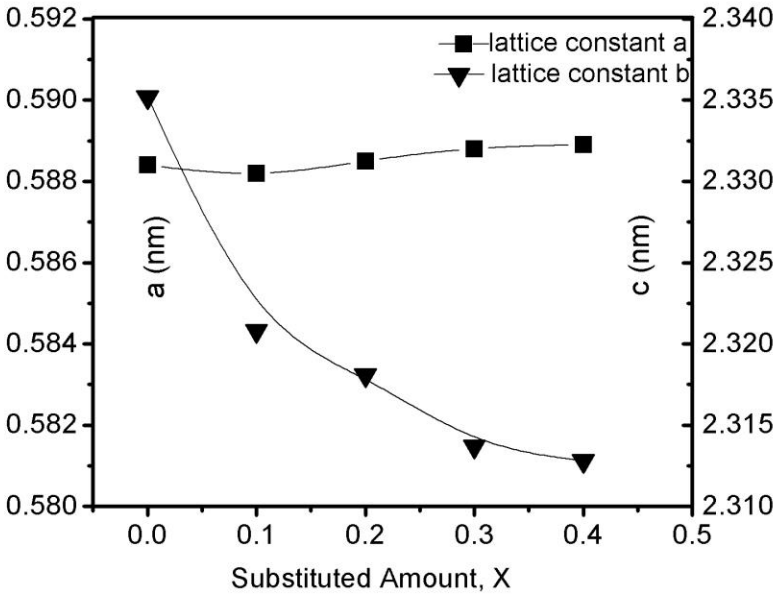

Fig. 2. Lattice constant as a function of *x* for $BaFe_{12-x}Cr_xO_{19}$ ceramics

Morphology Properties

A comparison of the microstructures in spruce charcoal and spruce-templated $BaFe_{11.8}Cr_{0.2}O_{19}$ ceramics after sintering at 1000 °C clearly showed that the original cellular anatomy of the spruce template was retained in the $BaFe_{12-x}Cr_xO_{19}$ product (Fig. 3). Because of anisotropic thermal contraction resulting from drying and calcination, some cracks were created in the cell walls. Compared with the pores in spruce charcoal (Fig. 3(a)), the pores in Fig. 3(c) arose from the same original cells, *i.e*., tracheid, which

were reduced from 40 to 55 μm to about 30 to 45 μm in diameter. The smaller pores were enclosed in a thin layer of cell wall, which had a thickness of 1 to 2 μm (Fig. 3d).

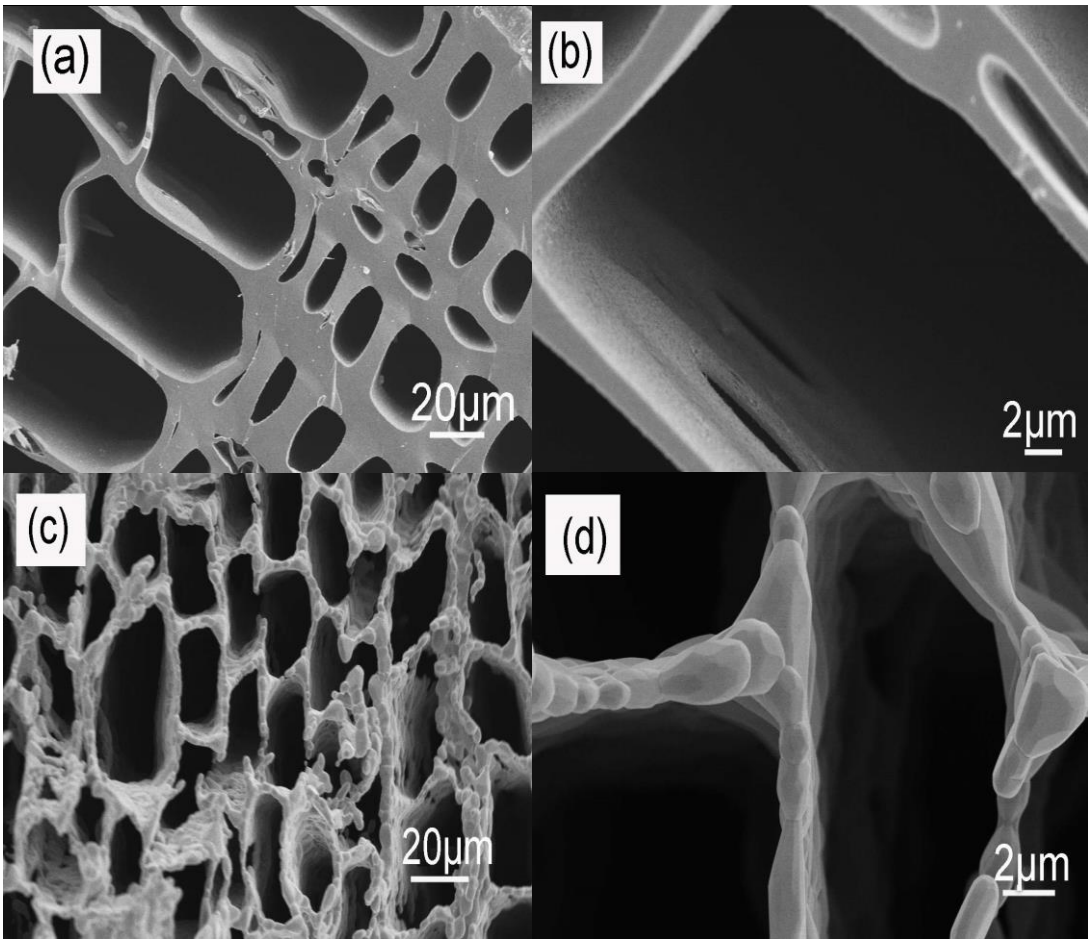

Fig. 3. SEM images of (a) and (b), spruce charcoal after sintering at 1000 °C in N_2; (c) and (d), spruce-templated $BaFe_{11.8}Cr_{0.2}O_{19}$ ceramic after sintering at 1000 °C in O_2

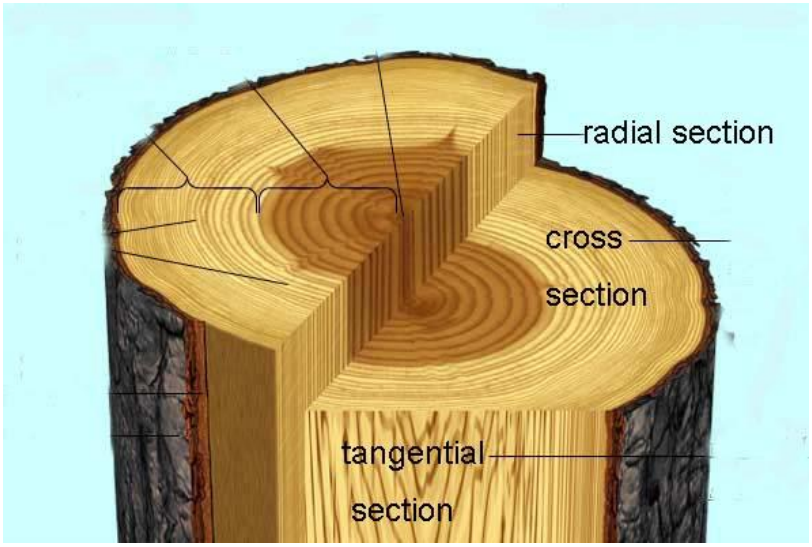

Fig. 4. Principle sections used for describing the physical properties of wood

Magnetic Properties

The conventional labeling of the principle sections of wood is shown in Fig. 4. To investigate the influence of anisotropy in the spruce template on the magnetic properties of biomorphic ceramics, the three directions were defined as follows: A, vibration of MPMS parallel to the cross-section; B, vibration of MPMS parallel to the radial section, and C, vibration of MPMS parallel to the tangential section. The biomorphic, $BaFe_{12-x}Cr_xO_{19}$ ceramics were divided into cubes of 4 × 4 × 4 mm^3 and measured for saturation magnetization (M_s) and coercivity (H_c) along the three directions (Table 1). Figure 5 shows the hysteresis loops in the three directions for the $BaFe_{11.8}Cr_{0.2}O_{19}$ ceramics after sintering at 1000 °C.

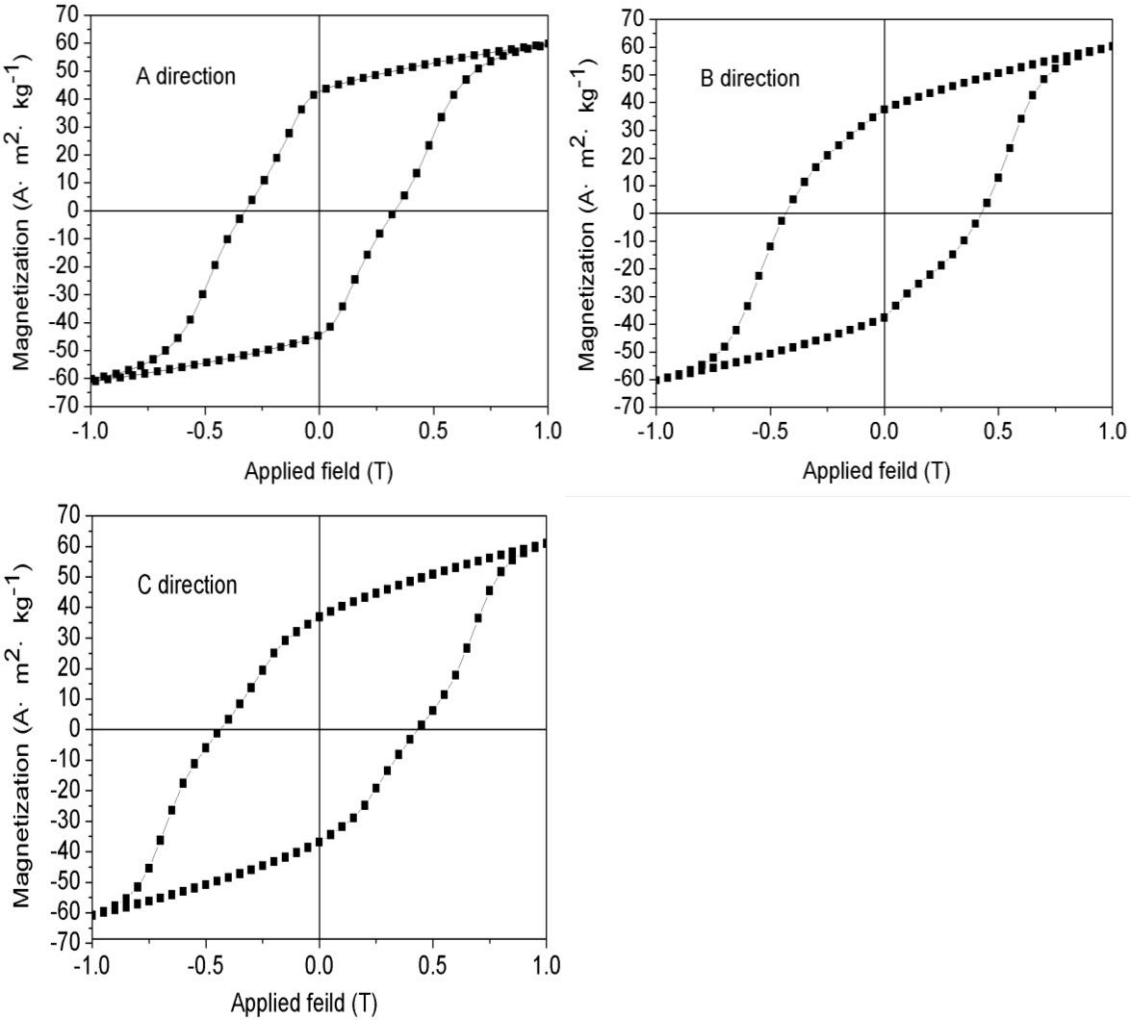

Fig. 5. The hysteresis loops in A, B, and C directions of $BaFe_{11.8}Cr_{0.2}O_{19}$ ceramic after sintering at 1000 °C

As *x* increased, the saturation magnetization increased initially to a maximum value at $x = 0.2$ and then declined in the three directions. This result suggested that low levels of Cr^{3+} doping ($x \leq 0.2$) improved the saturation magnetization of barium ferrite. The magnetic moment, as shown in the formula for BaM hexaferrite, was determined as the algebraic sum of magnetic moments of irons in different positions as follows (Chawla *et al*. 2014),

$$M = M(12k + 2b + 2a)\uparrow - M(4f_1 + 4f_2)\downarrow \quad (2)$$

where M is magnetic moment and 12k, 2b, 2a, 4f_1, and 4f_2 are five substitutional sites for iron in the hexagonal structure of BaM ferrite. The sites of 12k, 2a, and 2b have upward spin, while the 4f_1 and 4f_2 sites have downward spin directions.

Table 1. Magnetic Data of $BaFe_{12-x}Cr_xO_{19}$ Ceramics after Sintering at 1000 °C

x	M_{sA} ($A \cdot m^2 \cdot kg$)	M_{sB} ($A \cdot m^2 \cdot kg^{-1}$)	M_{sC} ($A \cdot m^2 \cdot kg^{-1}$)	H_{cA} ($kA \cdot m^{-1}$)	H_{cB} ($kA \cdot m^{-1}$)	H_{cC} ($kA \cdot m^{-1}$)
0	55.2	54.8	55.3	438.0	481.7	485.8
0.1	57.1	57.3	56.9	425.7	462.8	468.7
0.2	61.2	60.8	61.4	412.9	453.8	450.7
0.3	56.2	56.1	56.4	399.6	436.8	438.8
0.4	54.8	54.6	54.5	384.8	422.8	420.8

When Cr^{3+} replaced Fe^{3+} in the barium ferrite sublattice, it preferentially occupied the octahedral positions of 12k, 2a, and 4f$_2$. Mossbauer spectrum research has confirmed that Cr^{3+} molecules are randomly distributed in the 12k, 2a, and 4f$_2$ positions (Kuznetsov *et al.* 1999). Because the magnetic moment of Cr^{3+} (3μ_B) was less than the magnetic moment of Fe^{3+} (5μ_B), the number of Cr^{3+} doping in 4f$_2$ (spun down) was more than the number of Cr^{3+} doping in 2a (spun up), which lead to an increase in saturation magnetization in low Cr^{3+} content (Fang *et al*. 2005). The M_s values changed very little in the A, B, or C directions at the same doping content, which indicated that the saturation magnetization of $BaFe_{12-x}Cr_xO_{19}$ ceramics was not related to the anisotropy of wood (Li *et al*. 2012).

The data in Table 1 show that the coercivity in the three directions decreased with increasing x value. The decreased coercivity can be explained by two factors. For a uniaxial hexagonal compound, the anisotropic field (H_a) is expressed as follows (Ghasemi and Morisako 2008),

$$H_a = \frac{2k_1}{M_s} \quad (3)$$

where k_1 is the magneto-crystalline anisotropy constant and Ms is the saturation magnetization constant. Equation 3 indicates that a decrease in H_a is caused by a decrease in k_1. This result is consistent with experiments using $SrFe_{12-x}(ZnTi)_xO_{19}$ (Fang *et al*. 2001). Secondly, the shape-anisotropy ratio (c/a) decreased because the lattice constant (c) decreased with increasing chromium content; thus, coercivity decreased in the domain transfer process.

H_{cA} was far lower than H_{cB} (or H_{cC}) under the same doping ratios (Table 1). This result was primarily associated with structural anisotropy in the multilayer wall structure, which leads to decreased H_{cA}. Multilayered cell wall-film structures have a parallel arrangement, where the A direction is parallel to the film surface and the coercivity in the A direction is lower than the coercivity vertical to the A direction (Feng 2002).

CONCLUSIONS

1. The sol-gel method was used to prepare biomorphic $BaFe_{12-x}Cr_xO_{19}$ ceramics molded from spruce sapwood. SEM images showed that the barium ferrite was retained in the compound wall structure of the spruce wood. XRD analysis confirmed the formation of single-phase, hexagonal structures without impurities or secondary-phases.
2. The saturation magnetization changed very little in the cross-section, radial, or tangential directions at the same doping content, which indicated that the saturation magnetization of $BaFe_{12-x}CrxO_{19}$ ceramic was not related to wood anisotropy. The saturation magnetization first increased and then decreased with increasing Cr^{3+} concentration, suggesting that low levels of Cr^{3+} doping ($x \leq 0.2$) improve the saturation magnetization of barium ferrite. The coercivity in the three directions decreased with increasing *x*-value.

ACKNOWLEDGEMENTS

This work was financially supported by the National Key Technology R&D Program in the 12th five-year plan of China (No. 2014BAK09B03).

REFERENCES CITED

Birol, H., Rambo, C. R., Guiotoku, M., and Hotza, D. (2013). "Preparation of ceramic nanoparticlesvia cellulose-assisted glycine nitrate process: A review," *RSC Advanced* 3(9), 2873-2884. DOI: 10.1039/c2ra21810k

Chawla, S. K., Mudsainiyan, R. K., Meena, S. S., and Yusuf, S. M. (2014). "Sol–gel synthesis, structural and magnetic properties of nanoscale M-type barium hexaferrites BaCoxZrxFe(12−2x)O19," *Journal of Magnetism and Magnetic Materials* 350, 23-29. DOI:10.1016/j.jmmm.2013.09.007

Durmus, Z., Durmus, A., and Kavas, H. (2014). "Synthesis and characterization of structural and magnetic properties of graphene/hard ferrite nanocomposites as microwave-absorbing material," *Journal of Materials Science* 50(3), 1201-1213. DOI: 10.1007/s10853-014-8676-3

Fang, Q. Q., Jiao, Y. F., Li, R., Wang, J. Z., and Chen, H. (2005). "Studies on structure and magnetic properties of uniaxial M-type $SrFe_{12-x}Cr_xO_{19}$ hexaferrite nanocrystalline," *Acta Physica Sinica* 54(4), 1826-1830. DOI: 10.7498/aps.54.1826

Fang, Q. Q., Liu, Y. M., Yin, P., and Li, X. G. (2001). "Magnetic properties and formation of Sr ferrite nanoparticle and Zn, Ti/Ir substituted phases," *Journal of Magnetism and Magnetic Materials* 234(3), 366-370. DOI:10.1016/S0304-8853(01)00428-0

Feng, J. (2002). "Ba ferrite films with high coercivity and large squareness for perpendicular magnetic recording," *Acta Physica Sinica* 51(8), 1841-1845. DOI: 10.7498/aps.51.1841

Ghasemi, A., and Morisako, A. (2008). "Static and high frequency magnetic properties of Mn-Co-Zr substituted Ba-ferrite," *Journal of Alloys and Compounds* 456(1-2), 485-491. DOI: 10.1016/j.jallcom.207.02.101

Gordani, G. R., Ghasemi, A., and Saidi, A. (2014). "Enhanced magnetic properties of substituted Sr-hexaferrite nanoparticles synthesized by co-precipitation method," *Ceramics International* 40(3), 4945-4952. DOI: 10.1016/j.ceramint.2013.10.096

Hosseini, S. H., Asadnia, A., and Moloudi, M. (2015). "Preparation and electromagnetic wave absorption hard–soft Ba ferrite/polypyrrole core–shell nanocomposites," *Materials Research Innovations* 19(2), 107-112. DOI: 10.1179/1433075X14Y.0000000221

Hübert, T., Unger, B., and Bücker, M. (2009). "Sol–gel derived TiO_2 wood composites," *Journal of Sol-Gel Science and Technology* 53(2), 384-389. DOI:10.1007/s10971-009-2107-y

Katlakunta, S., Meena, S.S., Srinath, S., Bououdina, M., Sandhya, R. and Praveena, K. (2015). "Improved magnetic properties of Cr^{3+} doped $SrFe_{12}O_{19}$ synthesized via microwave hydrothermal route, " *Materials Research Bulletin* 63, 58-66. DOI:10.1016/j.materresbull.2014.11.043

Kaur, H., Singh, C., Kaur, R., Dhiman, T., and Narang, S. B. (2015). "Microwave and electrical properties of Co-Ti substituted M-type Ba hexagonal ferrite," *The European Physical Journal B* 88, 274-280. DOI: 10.1140/epjb/e2015-60475-8

Kuznetsov, M. V., Barquin, L. F., Pankhurst, Q. A., Parkin I. P. (1999). "Self-propagating high-temperature synthesis of barium–chromium ferrites $BaFe_{12}{-}x$ Cr_xO_{19} (0 6 x 6 6:0)," *Journal of Physics D: Applied Physics* 32(20), 2590-2598. DOI: 10.1088/0022-3727/32/20/302

Li, R., Liu, S., Gui, Y., Qian, L., Shu, Z., and Mei, L. (2012). "The magnetic properties of $Sr_{1-x}La_xFe_{12-x}Co_xO_{19}$ hexaferrite prepared from masson pine sapwood, " *Journal of Functional Materials* 21(43), 3014-3017.

Liu, Z., Fan, T. and Zhang, D. (2006). "Synthesis of biomorphous nickel oxide from a pinewood template and investigation on a hierarchical porous structure, " *Journal of the American Ceramic Society* 89(2), 662-665. DOI: 10.1111/j.1551-2916.2005.00741.x

Ohji, T., and Fukushima, M. (2012). "Macro-porous ceramics: Processing and properties," *International Materials Reviews* 57(2), 115-131. DOI:10.1179/1743280411Y.0000000006

Okada, K., Isobe, T., Katsumata, K.-i., Kameshima, Y., Nakajima, A., and MacKenzie, K. J. D. (2011). "Porous ceramics mimicking nature-preparation and properties of microstructures with unidirectionally oriented pores," *Science and Technology of Advanced Materials* 12(6), 064701. DOI:10.1088/1468-6996/12/6/064701

Ota, T., Takahashi, M., Hibi, T., and Ozawa, M. (1995). "Biomimetic process for producing SiC 'wood'," *Journal of the American Ceramic Society* 78(12), 3409-3411. DOI: 10.1111/j.1151-2916.1995.tb07988

Pullar, R. C., Marques, P., Amaral, J., and Labrincha, J. A. (2015). "Magnetic wood-based biomorphic $Sr_3Co_2Fe_{24}O_{41}$ Z-type hexaferrite ecoceramics made from cork templates," *Materials & Design* 82(5), 297-303. DOI:10.1016/j.matdes.2015.03.047

Qian, L., Li, R., Zhou, L., Liu, Y., Yu, M., Xiong, F., Liu, S., and Hao, X. (2015). "Preparation of biomorphic TiO_2 ceramics from rattan templates," *BioResources* 10(3), 4391-4402. DOI: 10.15376/biores.10.3.4391-4402

Töpfer, J., Seifert, D., Le Breton, J. -M., Langenhorst, F., Chlan, V., Kouřil, K., and Štěpánková, H. (2015). "Hexagonal ferrites of X-, W-, and M-type in the system Sr–Fe–O: A comparative study," *Journal of Solid State Chemistry* 226, 133-141. DOI:10.1016/j.jssc.2015.02.007

Van Opdenbosch, D., Kostova, M. H., Gruber, S., Krolikowski, S., Greil, P., and Zollfrank, C. (2010). "Replication of wood into biomorphous nanocrystalline Y2O3:Eu3+ phosphor materials," *Wood Science and Technology* 44(4), 547-560. DOI: 10.1007/s00226-010-0375-x

Article submitted: November 25, 2015; Peer review completed: February 6, 2016; Revised version received and accepted: March 2, 2016; Published: March 14, 2016.
DOI: 10.15376/biores.11.2.3937-3946